Influence of Nonlinear Blade Damping on Helicopter Ground Resonance Instability

D.M. Tang* and E.H. Dowell†
Duke University, Durham, North Carolina

The lagging motion of each helicopter blade is assumed to be of equal amplitude and equally apportioned phase, thus allowing a simplified analytical method to be used to calculate the ground resonance instability of a helicopter model with nonlinear dampers in both the landing gear and blades. The geometrical nonlinearities of the blade lag motion and the influence of initial disturbances on ground resonance instability are also discussed. Finally an experiment is carried out using a helicopter scale model. The experimental data agree well with analysis.

Nomenclature

d = slope, see Fig. 1b, 1/s
H, h_s = geometrical lengths of the model, see Fig. 1a, in.
I = mass moment of inertia of blade relative to drag hinge, lb-in.-s
J_x, J_z = mass moments of inertia of fuselage about X and Z axes, respectively, through A, lb-in.-s
J_0 = average mass moment of inertia of fuselage, $(J_x + J_z)/2$, lb-in.-s
K_x, K_z = spring coefficients of fuselage at landing gear, lb/in.
L = distance from the axis of rotation center to drag hinge center, in.
m_{hx}, m_{hz} = nondimensional hydraulic damping coefficients in landing gear
$m_{dx} m_{dz}$ = dry friction damping coefficients in landing gear, 1/s
m_b = mass of the blade, lb-s-in.
m_0 = damping moment coefficient, see Fig. 1b
m_{db} = dry friction damping coefficient in blade damper, 1/s
N = number of blades
n_b = equivalent viscous damping coefficient of blade, 1/s
n_x, n_z = equivalent viscous damping coefficients of fuselage, 1/s
P = frequency parameter, $\Omega - \lambda$, Hz
P_x, P_z = natural frequencies of fuselage, Hz
R = blade radius, in.
S = static mass moment relative to drag hinge, lb-s.
t, T = time, s
θ_x, θ_z = angular motions of fuselage about X and Z axes, respectively
θ_{x0}, θ_{z0} = angular amplitudes of fuselage about X and Z axes, respectively
ψ_k = azimuthal angle, deg
ξ_k, ξ_0 = angular deflection and amplitude, respectively, of kth blade; $\tilde{\xi}_0 = 3SH\xi_0/2J_0$, see Eq. (7)
ν_0 = nondimensional blade parameter, $\sqrt{LS/I}$
Ω = rotor speed, Hz
σ = nondimensional hydraulic damping coefficient in blade damper; $\tilde{\sigma} = 2J_0\sigma/3SH$, see Eq. (7)
ϕ_0, ϕ_1 = phase difference of ξ_k with respect to θ_x, for hydraulic and dry friction damping in the blade, respectively, rad
ϕ_z = phase difference of θ_z with respect to θ_x, rad
λ = oscillation frequency of the fuselage, Hz
$\epsilon_1, \epsilon_2, \epsilon_3$ = nondimensional parameter of mass moment of inertia, $\epsilon_1 = 3S^2H^2/2J_0I$, $\epsilon_2 = J_0/J_x$, and $\epsilon_3 = J_0/J_z$, respectively

Superscripts

$(\dot{})$ = d/dt
$()'$ = $d/d\tau$

Introduction

GROUND resonance is a potentially destructive instability that can occur in helicopters with fully articulated or soft in-plane rotors. The nonlinear dynamics of a helicopter model with nonlinear dampers in the landing gear have been analyzed and discussed in a previous work.[1] See Refs. 1 and 2 for a discussion of related work and earlier literature. The practical design of a helicopter requires sufficient damping in both the blades and landing gear to prevent this type of instability. In some cases, the use of a nonlinear damper in the blades can eliminate the need for damping in the landing gear, such that the damping provided by a conventional skid gear will be sufficient.

Addition of nonlinear damping in the blades complicates the equations of blade lagging motion by introducing periodic coefficients. The well-known Coleman transformation,[3] often used in a linear rotor system, does not apply to the present case. Tongue[2] has provided an iterative method to deal with the nonlinearity in the rotor system which is also used here.

In the present paper, the lagging motion of each blade is assumed be of equal amplitude and equally apportioned phase, thus allowing a simplified analytical method to be used. Numerical simulations that do not invoke this assumption indicate that it and the simplified method are satisfactory for hydraulic resistance, dry friction, or a combination of hydraulic and linear force-velocity damping characteristics.

In addition to including damping nonlinearities in both the fuselage and blades, also considered is the influence of including all second-order terms in the rotor system on the ground resonance instability. Another interesting question considered is: How large must the initial disturbance be to induce unstable motion if the blades have dry friction damping and the disturbance acts only on the fuselage?

Lastly, a discussion of an experimental investigation carried out on a helicopter model is presented; see Ref. 4 for a complete description. Generally good agreement between theoretical and experimental results is found.

Received Feb. 1, 1985; revision received Aug. 5, 1985.

*Visiting Scholar, Department of Mechanical Engineering and Materials Science; Lecturer, Nanjing Aeronautical Institute, China.
†Dean, School of Engineering.

Simplified Method of Nonlinear Analysis

A sketch of the helicopter model is shown in Fig. 1a. The damping characteristics assumed is that the nondimensional blade damping moment m_1 is approximately proportional to the angular velocity squared of the blade lagging motion (hydraulic), is a dry friction damping moment m_2 or a combined quadratic-linear damping moment m_3, see Fig. 1b. These are represented as follows:

$$m_1 = \sigma\dot{\xi}_k|\dot{\xi}_k| \qquad m_2 = m_{db}\,\mathrm{sign}\dot{\xi}_k$$

$$m_3 = \sigma\dot{\xi}_k|\dot{\xi}_k|; \qquad \dot{\xi}_k < \sqrt{m_0/\sigma}$$

$$= d(\dot{\xi}_k - \sqrt{m_0/\sigma}) + m_0; \qquad \dot{\xi}_k > \sqrt{m_0/\sigma}$$

The equations of motion for the system that includes both a nonlinear landing gear damper and a nonlinear blade damper can be represented as follow:[1,2]

$$\ddot{\xi}_k + 2n_b\dot{\xi}_k + m_i + \nu_0^2\Omega^2\xi_k = \frac{SH}{I}(\ddot{\theta}_x\sin\psi_k - \ddot{\theta}_z\cos\psi_k) \tag{1}$$

$$\ddot{\theta}_x + 2n_x\dot{\theta}_x + m_{hx}\dot{\theta}_x|\dot{\theta}_x| + m_{dx}\mathrm{sign}\dot{\theta}_x + P_x^2\theta_x$$

$$= \frac{HS}{J_x}\sum_{k=1}^{N}\left[(\ddot{\xi}_k - \Omega^2\xi_k)\sin\psi_k + 2\Omega\dot{\xi}_k\cos\psi_k\right] \tag{2}$$

$$\ddot{\theta}_z + 2n_z\dot{\theta}_z + m_{hz}\dot{\theta}_z|\dot{\theta}_z| + m_{dz}\mathrm{sign}\dot{\theta}_z + P_z^2\theta_z$$

$$= -\frac{HS}{J_z}\sum_{k=1}^{N}\left[(\ddot{\xi}_k - \Omega^2\xi_k)\cos\psi_k - 2\Omega\dot{\xi}_k\sin\psi_k\right] \tag{3}$$

where $i = 1$, 2, or 3.

In order to solve nonlinear equations with periodic coefficients in the rotor system, a simplifying assumption is adopted herein. Verification of this assumption by numerical simulation solutions of Eqs. (1-3) is discussed more fully in Ref 5. Only a brief discussion will be given subsequently.

It is assumed that one can express ξ_k as

$$\xi_k = \xi_0\sin\left[(\Omega - \lambda)t + \frac{2\pi}{N}k + \phi_0\right] \tag{4}$$

Let

$$\theta_x = \theta_{x0}\cos\lambda t \tag{5}$$

and

$$\theta_z = \theta_{z0}\cos(\lambda t - \phi_z) \tag{6}$$

The next step will be to construct a describing function approximation for the damper characteristics of the blades:

$$m_1 = \xi_0^2(\Omega - \lambda)^2\frac{8\sigma}{3\pi}\cos\left[(\Omega - \lambda)t + \frac{2\pi k}{N} + \phi_0\right]$$

$$m_2 = m_{db}\frac{4}{\pi}\cos\left[(\Omega - \lambda)t + \frac{2\pi k}{N} + \phi_1\right]$$

$$m_3 = \frac{2}{\pi}\left\{\sigma\xi_0^2(\Omega - \lambda)^2\left[\frac{4}{3} - \frac{3}{2}\cos\theta_0 + \frac{1}{6}\cos(3\theta_0)\right]\right.$$

$$\left. + 2m_0\cos\theta_0 + \frac{d}{2}[\pi - 2\theta_0 - \sin(2\theta_0)]\xi_0(\Omega - \lambda)\right\}$$

where

$$\theta_0 = \sin^{-1}\sqrt{m_0/\sigma\xi_0^2(\Omega - \lambda)^2}$$

As an example, take $m_i = m_1$, and a final simplified formula is obtained. For $m_i = m_2$ and $m_i = m_3$ a similar treatment can be carried out.

Substitute Eq. (4) into Eq. (1), multiply the new equation by $\sin\psi_k$, sum these equations, and note the following trigonometric identities:

$$\sum_{k=1}^{N}\sin\psi_k\cos\psi_k = 0, \qquad \sum_{k=1}^{N}\sin^2\psi_k = \frac{N}{2}$$

Substitute Eqs. (5) and (6) into Eqs. (2) and (3), then consider a describing function approximation for the damper characteristics of the fuselage as

$$\mathrm{sign}\dot{\theta}_x = -\frac{4}{\pi}\sin\lambda t$$

$$\dot{\theta}_x|\dot{\theta}_x| = -\frac{8}{3\pi}\theta_{x0}^2\lambda^2\sin\lambda t$$

$$\mathrm{sign}\dot{\theta}_z = -\frac{4}{\pi}\sin(\lambda t - \phi_z)$$

$$\dot{\theta}_z|\dot{\theta}_z| = -\frac{8}{3\pi}\theta_{z0}^2\lambda^2\sin(\lambda t - \phi_z)$$

Using the harmonic balance method, six simultaneous nonlinear algebraic equations are derived to determine the quantities $\tilde{\xi}_c$, $\tilde{\xi}_s$, $\tilde{\theta}_{x0}$, $\tilde{\theta}_{zc}$, $\tilde{\theta}_{zs}$, and λ. For a detailed derivation, see Ref. 5. The final equations can be expressed as follows:

$$(\nu_0^2\Omega^2 - P^2)\tilde{\xi}_c - \left(2n_bP + \tilde{\xi}_0P^2\frac{8\tilde{\sigma}}{3\pi}\right)\tilde{\xi}_s + \frac{1}{2}\epsilon_1\lambda^2 \times (\tilde{\theta}_{x0} + \tilde{\theta}_{zs}) = 0$$

$$(\nu_0^2\Omega^2 - P^2)\tilde{\xi}_s + \left(2n_bP + \tilde{\xi}_0P^2\frac{8\tilde{\sigma}}{3\pi}\right)\tilde{\xi}_c - \frac{1}{2}\epsilon_1\lambda^2\tilde{\theta}_{zc} = 0$$

$$(-\lambda^2 + P_x^2)\tilde{\theta}_{x0} + \epsilon_2\lambda^2\tilde{\xi}_c = 0$$

$$2n_x\lambda\tilde{\theta}_{x0} + \frac{8}{3\pi}m_{hx}\lambda^2\tilde{\theta}_{x0}^2 + \frac{4}{\pi}m_{dx} - \epsilon_2\lambda^2\tilde{\xi}_s = 0$$

$$(-\lambda^2 + P_z^2)\tilde{\theta}_{zc} + (2n_z\lambda + \frac{8}{3\pi}m_{hz}\lambda^2\tilde{\theta}_{z0} + \frac{4}{\pi}m_{dz}/\tilde{\theta}_{z0})\tilde{\theta}_{zs} - \epsilon_3\lambda^2\tilde{\xi}_s = 0$$

$$(-\lambda^2 + P_z)\tilde{\theta}_{zs} - (2n_z\lambda + \frac{8}{3\pi}m_{hz}\lambda^2\tilde{\theta}_{z0} + \frac{4}{\pi}m_{dz}/\tilde{\theta}_{z0})\tilde{\theta}_{zc} + \epsilon_3\phi^2\tilde{\xi}_c = 0 \tag{7}$$

where

$$\tilde{\theta}_{x0} = \theta_{x0}, \qquad \tilde{\theta}_{z0} = \theta_{z0}$$

$$\tilde{\xi}_c = \tilde{\xi}_0\cos\phi_0, \quad \tilde{\xi}_s = \tilde{\xi}_0\sin\phi_0, \quad \tilde{\xi}_0 = \sqrt{\tilde{\xi}_c^2 + \tilde{\xi}_s^2}$$

$$\tilde{\theta}_{zc} = \tilde{\theta}_{z0}\cos\phi_z, \quad \tilde{\theta}_{zs} = \tilde{\theta}_{z0}\sin\phi_z, \quad \tilde{\theta}_{z0} = \sqrt{\tilde{\theta}_{zc}^2 + \tilde{\theta}_{zs}^2}$$

Numerical Solution Procedure and Results

The approximate solution method outlined in the previous section will now be demonstrated on a helicopter model with only one-degree-of-freedom fuselage motion.

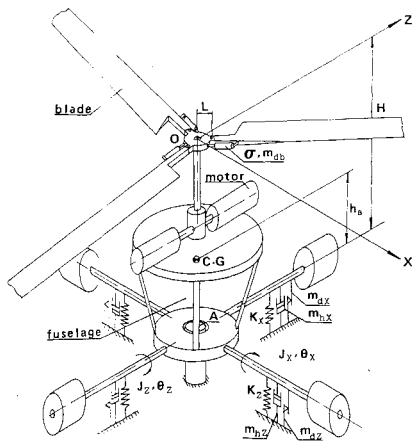

Fig. 1a Test model.

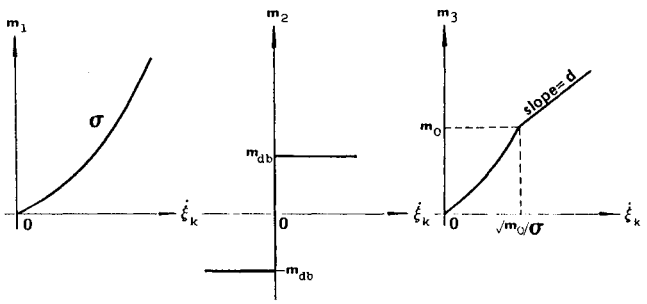

Fig. 1b Damping characteristics of blade damper.

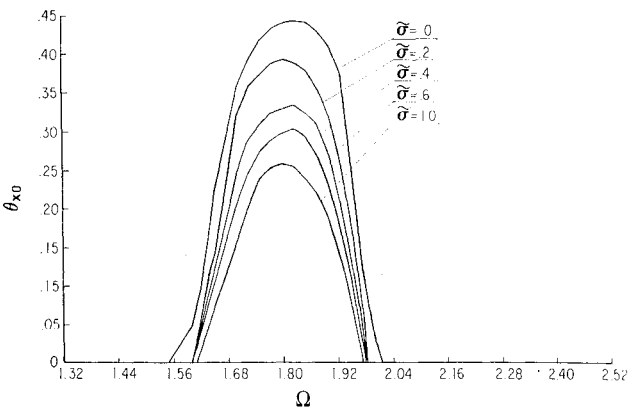

Fig. 2 Limit cycle amplitude vs rotor speed for various nonlinear blade damping levels.

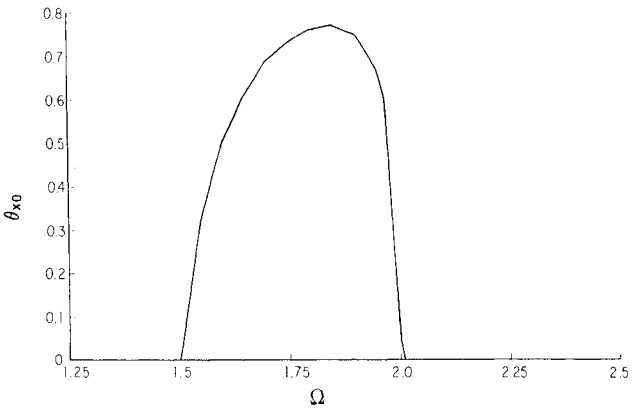

Fig. 3 Limit cycle amplitude vs rotor speed for $\tilde{\sigma}=1$, $m_{hx}=0$.

In Eqs. (7), the $\tilde{\theta}_{zs}$ and $\tilde{\theta}_{zc}$ will be eliminated, and the first four equations will remain. From the third equation of Eqs. (7), there is the relationship

$$\tilde{\xi}_c = -(-\lambda^2 + P_x^2)\tilde{\theta}_{x0}/\epsilon_2\lambda^2$$

Substituting for ξ_c into the remaining equations, three simultaneous nonlinear algebraic equations are derived for determining the quantities $\tilde{\theta}_{x0}$, λ, and $\tilde{\xi}_s$.

The Broyden method[6] was used to solve the preceding simultaneous equations. In summary, we chose an initial guess of $\tilde{\theta}_{x00}$, $\tilde{\xi}_{s0}$, and λ_0, and used an iterative process to satisfy the following equations:

$$f_1(\tilde{\theta}_{x0}, \tilde{\xi}_s, \lambda) = 0$$

$$f_2(\tilde{\theta}_{x0}, \tilde{\xi}_s, \lambda) = 0$$

$$f_3(\tilde{\theta}_{x0}, \tilde{\xi}_s, \lambda) = 0$$

To test the validity of the calculation results, numerical simulation integrations of the nonlinear equations of motion were performed; see the Appendix for details. The limit cycle amplitudes and oscillation frequencies found from the numerical integrations agreed well with the results of the preceding approximate procedure.

Figure 2 shows the limit cycle behavior for several nonlinear damping levels in the blades. The following model parameters are used for this example: $n_b = 0.03067$, $n_x = 0.0315$, $P_x = 1.03$, $m_{hx} = 0.5$, $m_{dx} = 0$, $\epsilon_1 = 0.244$, $\epsilon_2 = 1$. From the figure it is found that the maximum limit cycle amplitude occurs near the critical rotor speed[3] of the linear system. The curves have a shape similar to the figure without nonlinear blade damping, i.e., $\tilde{\sigma}=0$, but the response amplitude decreases as the nonlinear damping increases, and the instability region becomes narrower. Physically, the action of nonlinear blade damping is to increase the stability margin of the system, as well as to increase the equivalent nonlinear damping in the landing gear, but the addition of a nonlinear damper in the blades does not produce a qualitative difference.

Figure 3 shows the limit cycle behavior for given $\tilde{\sigma}=1.0$ and the nonlinear dampers in the landing gear removed. As compared with Fig. 2, it is found that a sufficient nonlinear damping level in the blades also can suppress the ground resonance instability or reduce the limit cycle amplitude response in the instability region. However the effectiveness of nonlinear blade damping is not as high as that of the nonlinear damping in the landing gear. In order to achieve the same stability margin, a higher nonlinear blade damping level is required.

Figure 4 shows the comparison of the simplified method and the numerical integration results for $\tilde{\sigma}=0.4$. Satisfactory agreement between the two methods is noted.

Figure 5 shows that the blades' motions tend to steady limit cycles when the rotor speed falls inside the unstable region at a rotor speed of 1.78 Hz. Some typical characteristics are found from these time histories.

1) At a given rotor speed, the limit cycle amplitude of individual blades is approximately identical.

2) When the motion of the blades tends to a limit cycle, the phase difference of response between two neighboring blades is nearly equal to $2\pi/3$.

In this paper, particular attention is also given to the full nonlinear equations in the case of $q=1$ in the Appendix. In addition to damper nonlinearities, the geometrical nonlinearities of the blade motion are included in the general equations when $q=1$. For $q=0$, these term are neglected. For the more complete nonlinear equations, thus far no one has

proposed a simplified method of solution. Here, in order to compare with the above simplified method and observe unstable phenomena in the case of large blade lag motion, a numerical integration is used to solve the full nonlinear equations for $q=1$ (see the Appendix). Figures 6 and 7 were obtained using $q=1$; all other results were for $q=0$.

Figure 6 shows the fuselage motion phase plane plots for various nonlinear blade damping levels at a rotor speed of 1.78 Hz. Figure 6a shows the phase plane plot without nonlinear damping in the blades. The fuselage motion becomes quite complex, the periodicity of the motion vanishes, and aperiodic (random-like) motion appears to occur. In addition to the main harmonic frequency component λ, which is nearly equal to the natural frequency of the fuselage, many noninteger harmonic components appear in the frequency spectrum, see Fig. 7, such as frequencies Ω, $2\Omega-\lambda$, 2Ω, $2\Omega+\lambda$, ... Moreover, the broadband frequency response, which occurs between the two dominant peak frequency components, suggests that the motion is chaotic. However, it is found that the lag motion angle is so large when this phenomenon occurs, that it makes its practical possibility doubtful. In fact, for an actual helicopter, this type of motion is unlikely to be observed, because the maximum allowable lag angle in the usual blade configuration is limited, or the blade tip has touched the ground due to large fuselage roll motion. As the nonlinear blade damping level increases, the fuselage roll motion approaches to a limit cycle, i.e., the random-like motion gradually tends to periodic motion, as shown in Fig. 6b. Moreover, the present solution for $q=1$ leads to the same results as those predicted by Eq. (1) for $q=0$. The reason is that as the damping level increases, the lag motion amplitude decreases, and the terms of second-order lag motion can be neglected. In our model instability experiment, random-like motion has never been found because the maximum allowable lag angle in the helicopter test model is equal to ± 20 deg.

Experimental Tests and Results

The experimental model used in the present study is a substantially modified version of that originally designed by Richard Bielawa of Rensselaer Polytechnic Institute, Troy, NY, for his work on ground resonance. The instrumentation and model configuration are the same as in Ref. 1. The model analyzed and tested in this paper is called the A-model. However, in the A-model, three nonlinear blade dampers are substituted for the linear dampers which were used in the study of Ref. 1.

The following test device was used to measure force characteristics. An electric motor with stepless variable speed provides a vibration source, and drives a cam that can generate a sine wave. The desired amplitude is obtained using the lever principle. A piezoelectric force transducer is mounted on the end of the damper piston. The output force signal is analyzed by a frequency spectral analyzer, HP3582A.

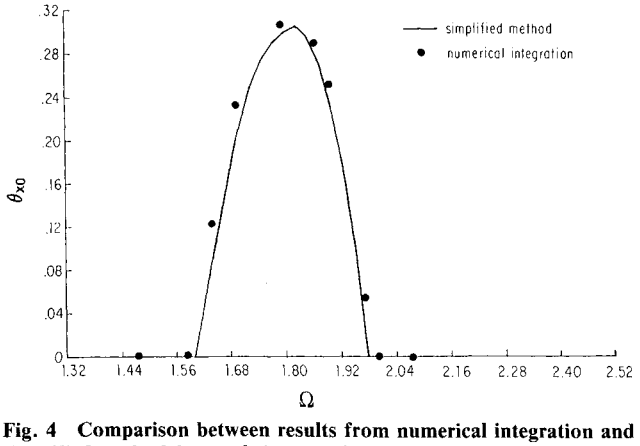

Fig. 4 Comparison between results from numerical integration and simplified method for $\tilde{\sigma}=0.4$, $m_{hx}=0.5$.

Figure 8 shows the velocity-force characteristic of the damper at two different fixed amplitudes. The curve indicates approximately three kinds of damping characteristics. In the very low region of velocity, the curve seems to be a straight line parallel to the horizontal axis (the values could not be measured accurately). It appears that there is a dry friction resistance in the damper caused by the rubber O-ring. In the region of velocity lower than 2.9 in.-s, the curve appears to have a quadratic characteristic. From the test, it is found that the force wave shape has a significant second-order harmonic component. In the higher region of velocity, the curve appears linear. The force wave shape is very nearly sinusoidal. Because the maximum lag motion angle is equal to ± 20 deg in the present scale model, the practical work region of the damper falls inside the quadratic limits when the unstable motion occurs. In the theoretical analysis used for comparison with experiment, the first two portions of the entire damper characteristic curve were modeled.

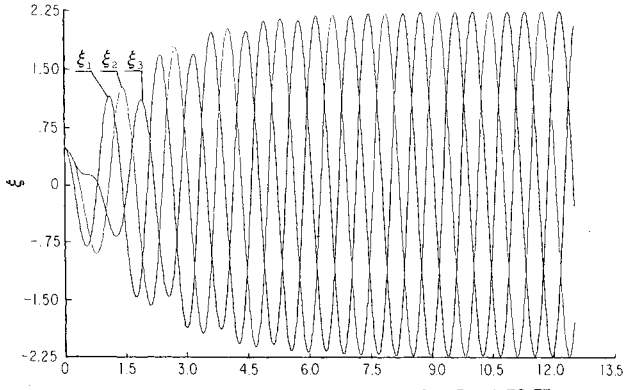

Fig. 5 Time history of blade motion for $\Omega=1.78$ Hz.

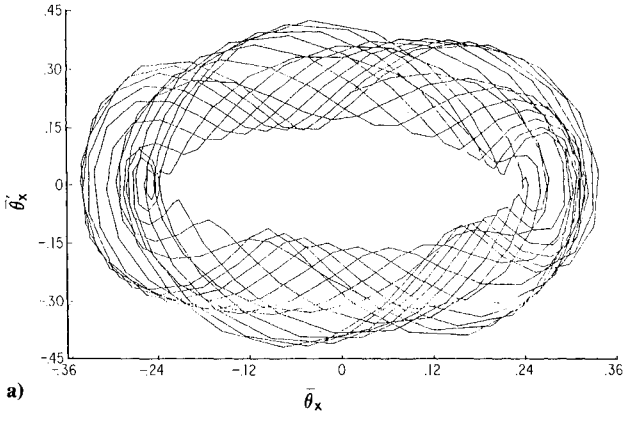

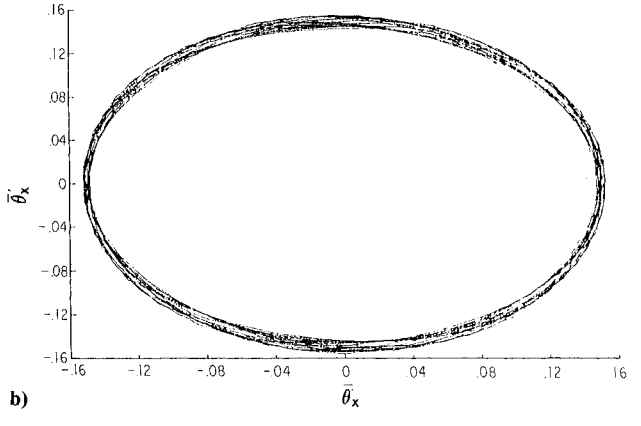

Fig. 6 Phase plane plot of fuselage motion for two different nonlinear blade damping levels for $m=0.5$, a) $\tilde{\sigma}=0$, b) $\tilde{\sigma}=0.4$.

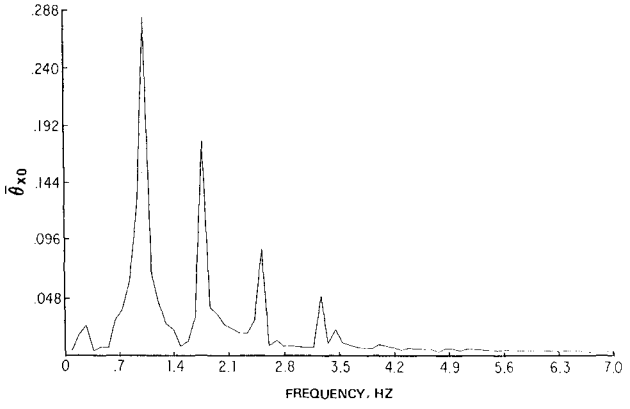

Fig. 7 Frequency spectrum for $\tilde{\sigma}=0$, $m_{hx}=0.5$.

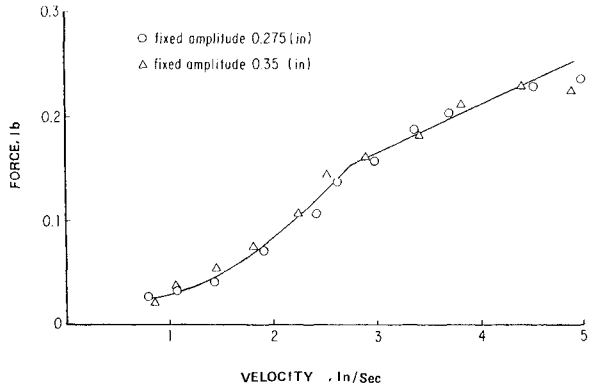

Fig. 8 Force vs velocity blade damper characteristic.

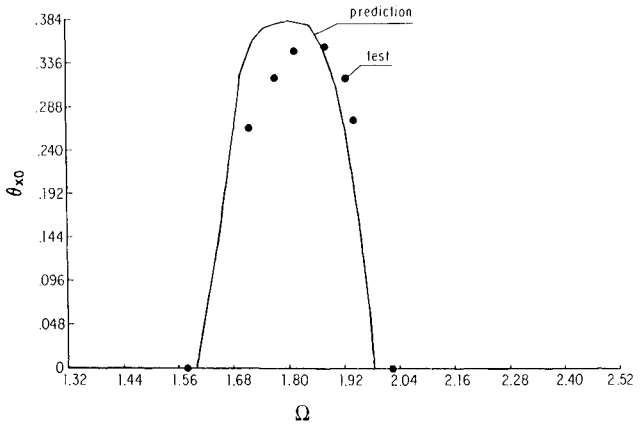

Fig. 9 Comparison of limit cycle behavior between calculation and test for amplitude vs rotor speed.

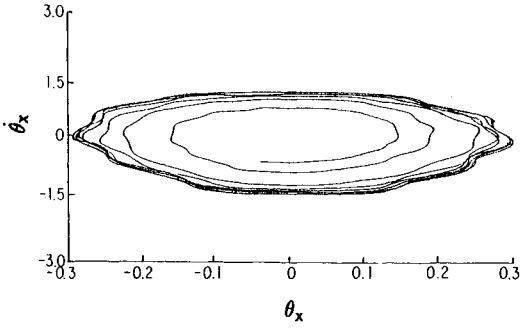

Fig. 10 Phase plane plot of fuselage motion from test for $\Omega=1.78$ Hz.

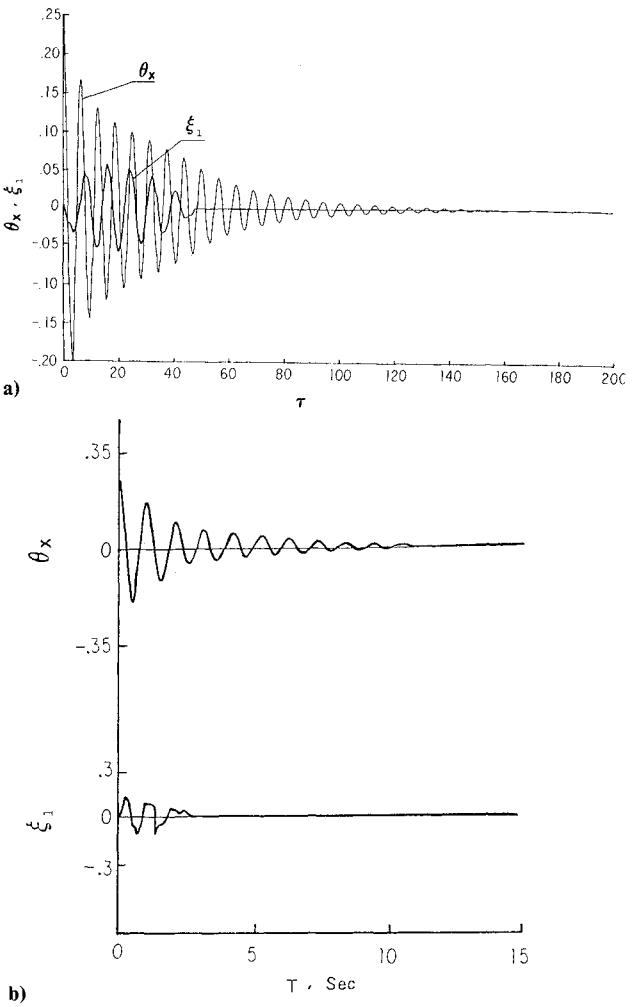

Fig. 11 Comparison between prediction and test under initial disturbance $\theta_x(0)=0.25$; a) prediction, b) test.

A stability test was accomplished by slowly varying the rotor speed until an instability was observed under a sufficiently large external disturbance. The signals are recorded simultaneously on a tape recorder. The limit cycle behavior, phase plane plots, and frequency spectrographs are analyzed by an HP3582A and plotted by an X-Y recorder.

Figure 9 shows the comparison between prediction and tests for the limit cycle behavior; the agreement is good. Figure 10 shows a phase plane plot of the measured fuselage motion. Although some higher-order harmonic components are included in the nearly elliptical curve, the steady-state limit cycle amplitude is very clear.

Figures 11-13 show the comparisons between prediction (Figs. 11a, 12a, and 13a) and test (Figs. 11b, 12b, and 13b) when different disturbances act on the fuselage at a rotor speed of 1.78 Hz. Although there are some quantitative differences, the general features of the test are well predicted by the calculation. However, when the initial disturbance is $\theta_x(0)=0.3$, the analytical and experimental results are shown to be opposite to each other, see Fig. 12. These differences mainly come from the quantitative error in the determination of dry friction damping in the blade damper and in the pin joint between the blades and the hub, because the dynamic dry friction damping coefficient could not be measured sufficiently accurately in the authors' test. The sensitivity to initial condition is primarily a result of dry friction damping.

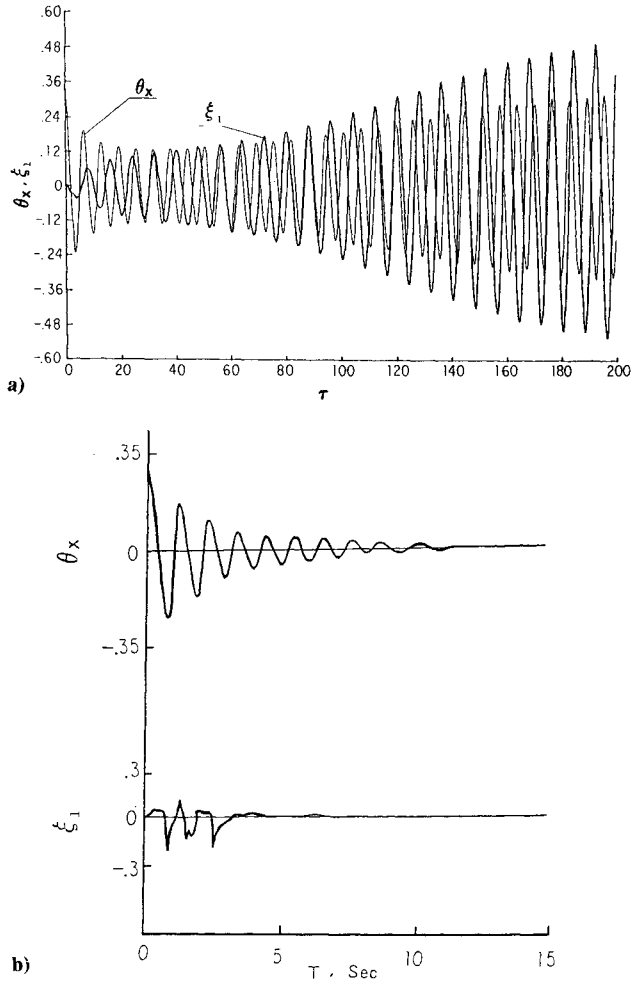

Fig. 12 Comparison between prediction and test under initial disturbance $\theta_x(0) = 0.3$; a) prediction, b) test.

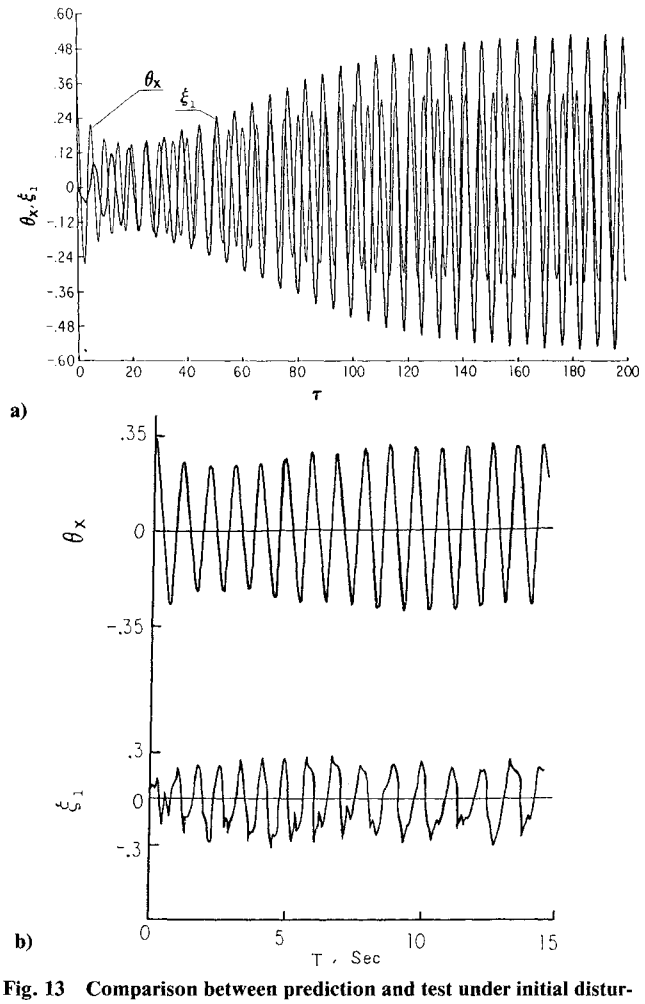

Fig. 13 Comparison between prediction and test under initial disturbance $\theta_x(0) = 0.35$; a) prediction, b) test.

Conclusions

1) The addition of a nonlinear hydraulic damper to the blades leads to a reduced response amplitude and an increased stability margin if there is a ground resonance instability. However, its action does not produce qualitatively different behavior from that of the nonlinear landing gear-linear blade configuration.[1] For some landing gear configurations, such as a conventional skid gear which is not able to provide sufficient damping to protect against ground resonance instability, the use of a nonlinear hydraulic blade damper may be quite beneficial. However this type of damper has a history of poor service life due to leakage and wear, and needs frequent maintenance.

2) The addition of dry friction damping to the blades is also advantageous. In some articulated helicopters, having only a dry friction damper in each blade is sufficient to avoid ground resonance instability.

3) The simplified theoretical method presented herein has been verified by numerical time-integration solutions. The satisfactory agreement between the results of the simplified method and numerical integration shows that the former method may be effective in evaluating the stability boundary and limit cycle amplitude of helicopters with nonlinear damping in both the blades and landing gear. Moreover, the theoretical results are in generally good agreement with the experiments reported herein.

Appendix: Determination of Limit Cycle Behavior by Numerical Time Integration

The full nonlinear equations of motion corresponding to the A-model including dry friction and hydraulic damping in the blades are[1,2]:

$$\ddot{\xi}_k + 2n_b\dot{\xi}_k + \sigma\dot{\xi}_k|\dot{\xi}_k| + m_{db}\text{sign}\dot{\xi}_k + \nu_0^2\Omega^2\xi_k = \frac{SH}{I}\ddot{\theta}_x\sin(\psi_k + \xi_k) \tag{A1}$$

$$\ddot{\theta}_x + 2n_x\dot{\theta}_x + m_{hx}\dot{\theta}_x|\dot{\theta}_x| + P_x^2\theta_x = \frac{HS}{J_x}\sum_{k=1}^{3}[\ddot{\xi}_k\sin(\psi_k + \xi_k) + (\Omega + \dot{\xi}_k)^2\cos(\psi_k + \xi_k)] \tag{A2}$$

where

$$\psi_k = \Omega t + 2\pi k/3$$

Let

$$\tau = P_x t, \quad \theta_x' = P_x\frac{d\theta_x}{d\tau}, \quad \xi_k' = P_x\frac{d\xi_k}{d\tau}, \quad \bar{\Omega} = \frac{\Omega}{P_x}, \quad \bar{n}_x = \frac{n_x}{P_x}$$

$$\bar{n}_b = \frac{n_b}{P_x}, \quad e = \frac{J_x}{HSm_{hx}}, \quad e_0 = \frac{H^2S^2}{IJ_x}, \quad \bar{\theta}_x = m_{hx}\theta_x$$

$$S_k = \sin\psi_k, \quad C_k = \cos\psi_k, \quad \bar{\sigma} = e\sigma, \quad \bar{m}_{db} = \frac{m_{db}}{e}, \quad \bar{\xi}_k = \frac{\xi_k}{e}$$

If all terms greater than second order are neglected, the nondimensional equations are

$$\bar{\xi}_k'' + 2\bar{n}_b\bar{\xi}_k' + (\bar{m}_{db+}\bar{\sigma}\bar{\xi}_k^2)\text{sign}\bar{\xi}_k' + \nu_0^2\bar{\Omega}^2\bar{\xi}_k = e_0\bar{\theta}_x''[S_k + qec_{kx}\bar{\xi}_k] \tag{A3}$$

$$\bar{\theta}_x'' + \bar{\theta}_x'|\bar{\theta}_x'| + 2\bar{n}_x\bar{\theta}_x' + \bar{\theta}_x = \sum_{k=1}^{3}[S_k(\bar{\xi}_k'' - \bar{\Omega}^2\bar{\xi}_k) + 2C_k\bar{\Omega}\bar{\xi}_k')] + qe\sum_{k=1}^{3}[-2\bar{\Omega}S_k\bar{\xi}_k'\bar{\xi}_k + C_k(\bar{\xi}_k''\bar{\xi}_k - \tfrac{1}{2}\bar{\Omega}^2\bar{\xi}_k^2 + \bar{\xi}_k'^2)] \tag{A4}$$

where $q = 0$ or 1 is a value to be chosen as discussed in the main text.

A vector of unknowns is defined as

$$Z^T = \{\bar{\xi}_1, \bar{\xi}_2, \bar{\xi}_3, \bar{\theta}_x\}$$

Equations (A3) and (A4) can be rewritten compactly as a matrix equation of fourth order.

$$[M]\{\ddot{Z}\} = \{B\} \tag{A5}$$

The mass matrix M is expressed as

$$[M] = \begin{bmatrix} 1 & 0 & 0 & -e_0R_1 \\ 0 & 1 & 0 & -e_0R_2 \\ 0 & 0 & 1 & -e_0R_3 \\ -R_1 & -R_2 & -R_3 & 1 \end{bmatrix}$$

$$\{B\} = -(\bar{m}_{db} + \bar{\sigma}\bar{\xi}_1'^2)\text{sign}\bar{\xi}_1' + \nu_0^2\bar{\Omega}^2\bar{\xi}_1 - (\bar{m}_{db} + \bar{\sigma}\bar{\xi}_2'^2)\text{sign}\bar{\xi}_2' + \nu_0^2\bar{\Omega}^2\bar{\xi}_2 - (\bar{m}_{db} + \bar{\sigma}\bar{\xi}_3'^2)\text{sign}\bar{\xi}_3' + \nu_0^2\bar{\Omega}^2\bar{\xi}_3 - \bar{\theta}_x'|\bar{\theta}_x'| - 2n_x\bar{\theta}_x' - \bar{\theta}_x - \sum_{k=1}^{3}(\bar{\Omega}^2\bar{\xi}_kS_k - 2\bar{\Omega}\bar{\xi}_k'C_k) + qe\sum_{k=1}^{3}(-2\bar{\Omega}\bar{\xi}_k\bar{\xi}_k'S_k - \tfrac{1}{2}\bar{\Omega}^2\bar{\xi}_k^2C_k + \bar{\xi}_k'^2C_k)$$

where

$$R_k = S_k + qeC_k\xi_k, \qquad k = 1,2,3$$

Decoupling Eq. (A5) and defining $y = \dot{z}$, the standard form for a set of first-order initial-value differential equations is obtained,

$$\dot{y}(t) = F(t,y) \quad \text{and} \quad y(t_0) = y_0$$

that is,

$$\{\dot{y}\} = [M]^{-1}\{B\} \tag{A6}$$

The fourth-order[7] Runge-Kutta method was used to solve the above equations and obtain limit cycle amplitudes through a phase plane plot.

Acknowledgment

This work was supported by the National Science Foundation under Grant MEA-8315193; Dr. Elbert Marsh, technical monitor.

References

[1]Tang, D.M. and Dowell, E.H., "Nonlinear Dynamics of a Helicopter Model in Ground Resonance," *Proceedings of the 2nd Decennial Specialists' Meeting on Rotorcraft Dynamics,* NASA Ames Research Center, Moffett Field, CA, Nov. 1984.

[2]Tongue, B.H., "Two Studies in Nonlinear Dynamical Systems," Ph.D. Thesis, Princeton University, Princeton, NJ, June 1983; also, "Limit Cycle Oscillations of a Nonlinear Rotorcraft Model," *AIAA Journal,* Vol. 22, July 1984, pp. 967-974.

[3]Coleman, R.P. and Feingold, A.M., "Theory of Self Excited Mechanical Oscillations of Helicopter Rotor with Hinged Blades," NACA Rept. 1352, Feb. 1957.

[4]Tang, D.M. and Dowell, E.H., "Nonlinear Dynamics of a Helicopter Model in Ground Resonance. Part 1: Analysis and Experiment on a Helicopter Model with Single Nonlinear Damper and Fuselage Motion," Duke University, Durham, NC, Engineering School Report, March 1984.

[5]Tang, D.M. and Dowell, E.H., "Nonlinear Dynamics of a Helicopter Model in Ground Resonance. Part 3: Nonlinear Dampers in the Landing Gear and Blades," Duke University, Durham, NC, Engineering School Report, Oct. 1985.

[6]Broyden, C.G., "A New Method of Solving Nonlinear Simultaneous Equations," *Computer Journal,* Vol. 12, No. 1, 1969.

[7]Conte, S.D. and de Boor, C., *Elementary Numerical Analysis,* 3rd Ed., McGraw-Hill Book Co., New York, 1980.